Ferroresonance Overvoltage Mitigation Using STATCOM for Grid-connected Wind Energy Conversion Systems

Mohamed I. Mosaad and Nehmdoh A. Sabiha

***Abstract*—We present the ferroresonance overvoltage mitigation concerning the power systems of the grid-connected wind energy conversion systems (WECSs). WECS is considered based on a doubly-fed induction generator (DFIG). Ferroresonance overvoltage associated with a single-pole outage of the line breaker is mitigated by fast regulating the reactive power using the static compensator (STATCOM). STATCOM controller is introduced, in which two incorporated proportional-integral (PI) controllers are optimally tuned using a modified flower pollination algorithm (MFPA) as an optimization technique. To show the capability of the proposed STATCOM controller in mitigating the ferroresonance overvoltage, two test cases are introduced, which are based on the interconnection status of the power transformer used with the grid-connected DFIGs. The results show that the ferroresonance disturbance can occur for the power transformers installed in the wind farms although the transformer terminals are interconnected, and neither side of the transformer is isolated. Furthermore, as a mitigation method of ferroresonance overvoltage, the proposed STATCOM controller succeeds in improving the system voltage profile and speed profile of the wind turbine as well as protecting the system components against the ferroresonance overvoltage.**

***Index Terms*—Ferroresonance overvoltage, doubly-fed induction generator (DFIG), static compensator (STATCOM), wind energy conversion system (WECS).**

I. Introduction

OWING to the fossil fuel and pollution problems as well as the clean and green generation, many renewable energy resources have been profusely integrated into the power grid [1]. Photovoltaic (PV), fuel cell, and wind energy conversion systems (WECSs) have been recently considered as the mostly used renewable energy resources [2], although they significantly affect the system reliability and voltage stability [3]. To overcome these problems associated with applying renewable energy sources, some control techniques and devices may be added to the power grid [4]. Generally, the interaction of the wind farm with the power grid should be dynamically investigated to avoid energy service interruption from these resources.

In the wind farms, the doubly-fed induction generator (DFIG) is one of the most important grid-connected energy conversion systems. However, they were sensitive to the wind speed variations, causing power fluctuations which badly affected the power quality [5]. With the high penetration of WECSs, some restrictions and solutions were proposed to support the ride-through capabilities under the abnormal power grid conditions such as the voltage sag/swell and faults [5]-[10]. In [9], flexible devices were added to regulate the active and reactive power flow between WECSs and the power grid. In [10], a superconductor was connected across the DC-link capacitor interconnected with the rotor- and grid-side converters of the DFIG to regulate the reactive power flow between the DFIG and the power grid. In [11], a unified power flow controller (UPFC) was used to improve the performance of the DFIG. A static compensator (STATCOM) was connected at the point of common coupling (PCC) between the DFIG and the power grid to improve the ride-through capabilities of the DFIG with either symmetrical or asymmetrical faults [12], [13]. All those mitigated disturbances, e. g., voltage sag and swell and faults, for the wind farm interconnected with the power grid were concerned by fundamental frequency and voltage disturbances. Also, the STATCOM applicability was ensured for the challenges of grid-connected wind farm operations.

Ferroresonance phenomena usually occurred due to the interaction between the system capacitances and non-linear inductances, in which they could be initiated by abnormal switching operations such as single-pole switching, transmission line clearing faults, and transformer energization. This contributed to slow transient overvoltage with non-sinusoidal or distortion waveforms affecting the power grid components. Therefore, the ferroresonance overvoltage mitigation was highly required to protect the power grid components against the damage. The mitigation could be classified according to the type of the considered transformer, i.e., voltage transformer or power transformer. For the voltage transformer, there were three main types of mitigation methods called active, passive, and control methods. These methods were widely covered in the literature [14]-[19]. However, all

Manuscript received: May 4, 2020; accepted: revised: June 24, 2020; September 4, 2020. Date of CrossCheck: September 4, 2020. Date of online publication: January 25, 2021.

M. I. Mosaad (corresponding author) is with Yanbu Industrial College, Yanbu Al Sinaiyah, Kingdom of Saudi Arabia (e-mail: m_i_mosaad@hotmail.com).

N. A. Sabiha is with the Electrical Engineering Department, Faculty of Engineering, Menofia University, 32511 Shebin Elkom, Egypt, and she is on leave to work at the Electrical Engineering Department, College of Engineering, Taif University, 21974 Taif, Kingdom of Saudi Arabia (e-mail: nehmdoh.sabiha@sh-eng.menofia.edu.eg).

DOI: 10.35833/MPCE.2020.000286

these methods were introduced to mitigate the ferroresonance associated with the voltage transformers containing light loads. There were few methods introduced to mitigate the ferroresonance overvoltage associated with the power transformers and more especially in the system of grid-connected wind farms. In [20], the dynamic interaction of the surge arrester within the non-linear inductance of the power grid was considered to limit the corresponding chaotic ferroresonance overvoltage. However, the energy absorption limit of the surge arrester was not evaluated, which could limit the capability of the surge arrester to suppress the ferroresonance overvoltage. In [21], solid-state current limiters associated with the reactor, resistor, and capacitor to mitigate both the fault and ferroresonance were designed as a dual function. In [22], the inductive superconducting fault current limiter was considered to mitigate the ferroresonance overvoltage. However, advanced technology is needed by the superconducting fault current limiters with an inductive behavior practically installed.

The ferroresonance overvoltage in wind farms occured due to the same reasons for the traditional power grids, where the elements of ferroresonance dynamic interactions were available such as the non-linear inductive elements and capacitances. The power transformers associated with the induction machines in the wind farms provided non-linear inductive elements. Besides, there were capacitive effects due to the overhead lines and underground cables distributed in the wind farms to transmit and collect the generated power toward the power grid. Furthermore, distributed reactive power supported capacitors might be installed, e.g., with the single-fed induction generators. In [23], further ferroresonance causes for the wind farms were addressed. In [24], the ferroresonance overvoltage were investigated considering energizing and de-energizing as the initialing conditions of the ferroresonance. The research was considered for different types of WECSs such as DFIG, squirrel cage induction generator, wound rotor induction generator, and permanent magnet synchronous generator. Ferroresonance overvoltage and its mode were addressed to ensure the ferroresonance occurrences in the wind farms.

We introduce a new application for exploiting STATCOM to mitigate the ferroresonance overvoltage of the grid-connected WECS based on DFIG. STATCOM is used to controllably inject or absorb reactive power to interact with the ferroresonance instance. Therefore, it mitigates the corresponding overvoltage due to ferroresonance occurrences. The considered STATCOM is controlled via two optimized proportional-integral (PI) controllers, which are optimized by the modified flower pollination algorithm (MFPA). Two different scenarios for the ferroresonance occurrence in the power grid including WECS, and the designed STATCOM are simulated using MATLAB/Simulink. One scenario is for the unloaded transformer, while the second one is for the loaded transformer. Based on the results, two different ferroresonance types are investigated, in which the second scenario produces higher overvoltage although the power transformer terminals at both sides are in service. Therefore, the reactive power participation of STATCOM is higher for the second scenario. Generally, the fast response from the STATCOM successfully mitigates the ferroresonance overvoltage and makes the system in safe operation.

II. System Description

The power system under study consists of six WECSs in DFIG-based wind farm, each rated in 1.5 MW, and is connected to the power grid via two transformers and transmission lines as shown in Fig. 1. As the power grid is at 120 kV level while the WECS is at 0.575 kV level, the ratings of the two considered transformers are 120 kV/25 kV and 25 kV/0.575 kV, respectively. As depicted in the zoomed part in Fig. 1, two voltage source converters (VSCs) coupled through DC capacitor are used for the WECS. The grid-side converter (GSC), which is the first VSC, is used to exchange the power between the power grid and the capacitor. The rotor-side converter (RSC), which is the second VSC, is used to feed the machine rotor. The generator data are presented in Appendix A.

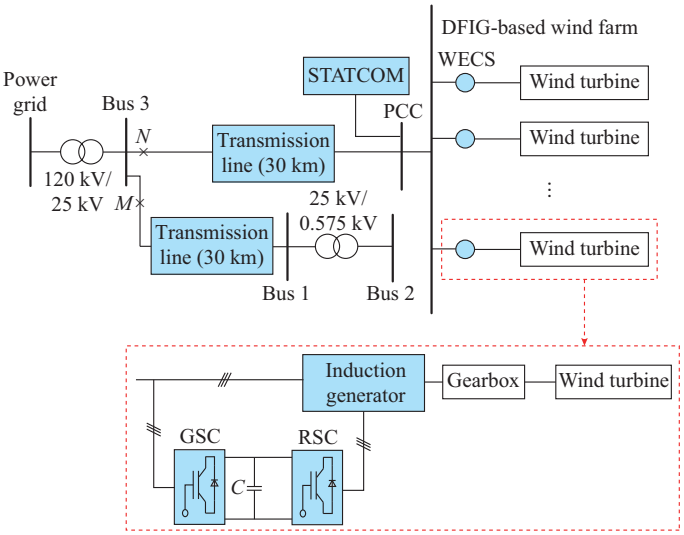

Fig. 1. Power system under study with ferroresonance.

In the DFIG-based wind farm, the distributed capacitances and non-linear inductances of the transformers and induction machines enhance the ferroresonance occurrence, even if the transformer is in service. In this paper, two different scenarios with ferroresonance overvoltage are considered when a single pole of the breaker opens. The first ferroresonance test case is the common one, where the power transformer is connected to the system through a 30 km transmission line, while its secondary side is isolated. In this test case, the ferroresonance phenomenon is stimulated by opening the pole of phase a for the breaker installed at point *M*, where the breaker pole stray capacitance is considered to be 0.01 μF, and the status of breaker installed at point *N* is closed. The other test case for simulating the ferroresonance is that the pole of phase a for the breaker at point *N* is opened as shown in Fig. 1. Note that there is a 30 km transmission line connecting the WECS to the power grid, and the three poles of the breaker at point *M* are open and isolated from this branch. In this test case, the transformer under ferroreso-

nance stress is in service, and there is no side isolated from the power grid. However, a single-pole opening of the breaker at node *N* causes the ferroresonance overvoltage as evaluated in Section IV.

The single-pole switching of the circuit breaker is considered in this paper. The equivalent analytical circuit is shown in Fig. 2 [25], where C_m and C_g are the mutual and grounding capacitances, respectively. As shown in Fig. 2, the network topology is changed across the non-linear inductance of the disconnected phase. The difference of the wind farm is that there are distributed underground cable capacitances and the non-linear inductance of the induction machine in parallel with the non-linear inductance of the transformer, which is shown as the dashed outlined non-linear inductance in Fig. 2.

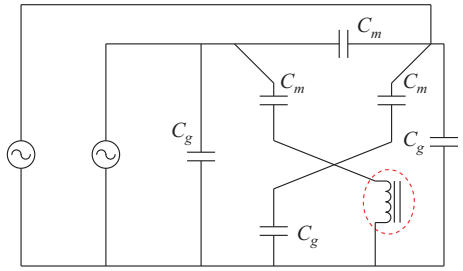

Fig. 2. Equivalent analytical circuit.

For the first ferroresonance scenario considered, the inductance is only for the transformer as it is isolated at the secondary side, which is shown in Fig. 1, where the single-pole switching is at point *M*. The second ferroresonance case is that the transformer is in service and the switching is at point *N*. However, the secondary side is not isolated but connected to DFIGs which contain induction machines with further non-linear magnetic circuits. Note that the machine rating is high, in which its participation is dynamically effective. The circuit in Fig. 2 has been usually utilized to analytically solve and find the ferroresonance overvoltage for single-pole switching. Instead of solving partial differential equations of the non-linear system, the other method is to simply represent the circuit using transient programs such as the electromagnetic transient program (EMTP) or MATLAB/Simulink, involving the system parameters and non-linearities. The advantage of the analytical circuit is to evaluate the effects of parameter variation on the ferroresonance performance [20], [25]. However, in this paper, the system is modeled in detail using MATLAB/Simulink. STATCOM is added to the power grid at PCC to regulate the reactive power flow and mitigate the ferroresonance overvoltage. Generally, STATCOM is installed at the point of connecting WECS to the power grid.

III. STATCOM Control

Using the STATCOM to enhance the integration of WECSs into the power grid provides a promising performance if they are properly controlled. Many controllers are introduced to drive the STATCOM as reported in [13], [26]-[28]. Regarding different types of controller, the classical PI controllers are used owing to their simplicity in the structure and implementation. Furthermore, the PI controllers are converted into adaptive controllers to drive the STATCOM for the WECS [6], [29].

Driving the STATCOM for the WECS to mitigate the ferroresonance is a non-linear problem. Accurate adjustment and tuning of the control parameters are needed to control the STATCOM using PI controllers. Evolutionary computing (EC) techniques are used for the optimal tuning of the PI control parameters in many applications. Genetic algorithm, particle swarm optimization, cuckoo search optimization, harmony search (HS), bacterial foraging optimization (BFO), MFPA, and electromagnetic field optimization (EFO) are utilized to find optimal PI control parameters for wide applications in the power grid [29]-[31].

By regulating the reactive power flows between the STATCOM and the power grid at PCC, the voltage at PCC can be controlled to mitigate the ferroresonance overvoltage for grid-connected wind farms. The ferroresonance phenomena cause a sudden increase in the system voltage instantaneously and in the form of repetitive transients and power frequency waveform distortion as the ferroresonance repeatedly occurs within positive and negative half-cycles.

A. STATCOM Controller

STATCOM is introduced to regulate the voltage and mitigate the effects of ferroresonance on the power grid. STATCOM is composed of two converters linked to DC capacitor C_1 as shown in Fig. 3(a). One converter is an uncontrolled rectifier (converter A), while the second one is a controlled DC-AC inverter (converter B). Through converter A, the power flows from the AC side to the DC side and vice versa for converter B. The controlled converter controls the charging/discharging of the capacitor based on the values of the PCC voltage and the STATCOM voltage V_{sa}. Under the normal operation condition, the STATCOM voltage lags the PCC voltage that leads to the power flow from the AC side to the DC side, consequently charging the capacitor to the maximum value of the grid voltage at PCC. If the capacitor voltage reaches the maximum value, there will be no power flow between the STATCOM and the power grid. Under abnormal operation conditions in the PCC voltage, the capacitor discharges and absorbs reactive power from the power grid.

The STATCOM is controlled by two PI controllers. The parameters of the two PI controllers are tuned by the optimization technique of MFPA. MFPA is used to minimize the integral of the square of error (ISE) between the reference voltage (1 p.u.) and the actual grid voltage at PCC. Then, the STATCOM successfully regulates the system voltage during the ferroresonance occurrence. The block diagram of the STATCOM controlled by the two PI controllers is shown in Fig. 3(b).

As shown in Fig. 3(b), the three-phase voltage V_a, V_b, V_c of PCC are sensed and converted by the *dq* frame into V_d and V_q. The other *dq* frame is to transform the three-phase current I_a, I_b, I_c into I_{qm}, in which I_d is set to be zero as there is no active power flow between the system and the STAT-

COM. The voltage magnitude at PCC V_m is calculated based on V_d and V_q, then it is compared with the reference voltage V_{ref} of 1 p.u.. The error between the reference and the voltage magnitude at PCC is e_v. Based on the difference between the voltage magnitude at PCC during the network disturbance such as ferroresonance and the reference voltage, e_v is used to stimulate controller A for updating the reference quadrature axis current as well as I_{qref}. Controller B is used to update the angle α, which is based on the difference between the updated reference quadrature current and the quadrature current component. This angle is added to the phase angle of PCC terminal voltage θ. Sinusoidal pulse width modulation (SPWM) is utilized to generate the switching pulses of the three-level inverter, driving the STATCOM to control the inverter voltage injected into the system based on α control [6].

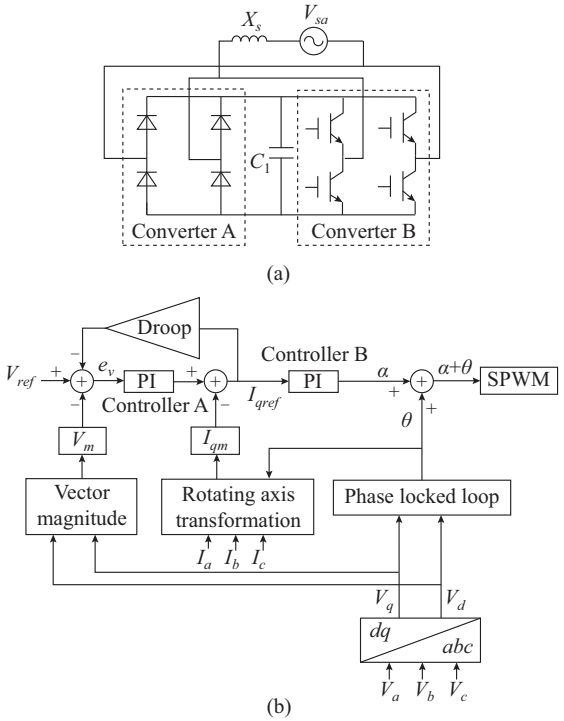

Fig. 3. Circuit and block diagram representation of STATCOM. (a) Single-phase STATCOM circuit. (b) Block diagram of STATCOM controlled by two PI controllers.

Controller A has two parameters K_{pA} and K_{IA}, and controller B has the other two parameters K_{pB} and K_{IB}. MFAP is used to optimally tune the parameters of two PI controllers while minimizing the objective function J, which is the integrated square error (ISE) function of $e_v(t)$ as:

$$J=\int_0^t (e_v(t))^2 \mathrm{d}t \tag{1}$$

The STATCOM is not used as an exact PCC voltage controller but it allows the voltage to vary in an accepted range proportional to the compensated current. Without allowing the voltage variation, a zero slope or droop is achieved which causes a poorly defined operation point and tendency to oscillation. In addition, the maximum capacitive and inductive ratings of the STATCOM could not be extended if the droop control is activated. The droop controller is used to allow the voltage to be more than the no-load voltage at inductive compensation and, conversely, for capacitive compensation as shown in Fig. 4. I_C abd I_L are the capacitive and inductive mode currents, respectively; and $I_{C,\max}$ and $I_{L,\max}$ are the maximum capacitive and maximum inductive mode currents, respectively.

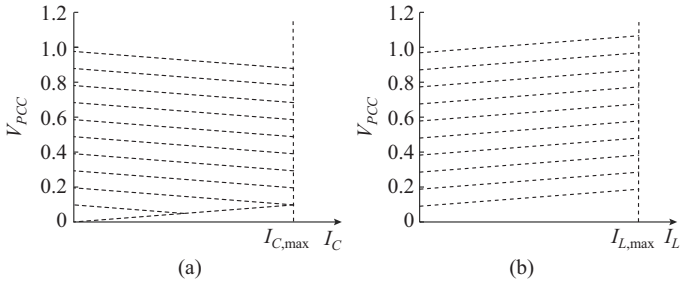

Fig. 4. Characteristics of current and voltage for STATCOM with droop controller. (a) Capacitive mode. (b) Inductive mode.

B. MFPA

MFPA is an amendment for the flower pollination algorithm (FPA) that depends on the application of clonal component animated from the clonal selection algorithm. Random walks are utilized to put in place of the Levy flights for their speedy convergence. The random walks are picked from a non-uniform distribution between 0 and 1. Besides, the local pollination is updated by step-size scaling factor y_2.

The pollination in flowers is a natural process, in which the pollinators are carried out by two types of carriers: biotic and abiotic. Biotic pollination refers to the process when the carriers are living organisms like insects. Abiotic pollination refers to the process when the carriers are non-living organisms such as air [31]. Some insects such as bees follow a Levy flight of the pollen to carry pollinators between the flowers and travel for long distances. If the bees carry the pollinators to the same flower, this is self-pollination, otherwise cross-pollination. Based on the four types of pollination introduced and with some combination, the biotic and cross-pollination are considered as global pollination, while the abiotic- and self-pollination are considered as the local pollination.

In the global type, the best generation is ensured by the ability of insects to travel for long distances, and the fittest is represented as J^x. J is the objective function to be minimized as defined in (1). Then, the flower fastness and the first rule can be mathematically expressed by:

$$x_i^{t+1}=x_i^t+y_1 L(J^x-x_i^t) \tag{2}$$

where x_i^t is a solution set at iteration t of the i^{th} current iteration that contains four variables of the two proposed PI controllers K_{pA}, K_{IA}, K_{pB}, K_{IB} for the STATCOM; x_i^{t+1} is the best solution at iteration $t+1$; y_1 is the step size scaling factor; and L is the pollination strength or the step size. The local pollination and flower constancy are formulated as:

$$x_i^{t+1}=x_i^t+y_2 L \in (x_i^t-x_k^t) \tag{3}$$

where $\in$ represents a uniform distribution between 0 and 1; x_k^t is the iteration k; and y_2 is the step size scaling factor.

The pollination may be local or global, then a switch probability P is used to discriminate them. The flowchart of MFPA optimization is illustrated in Fig. 5.

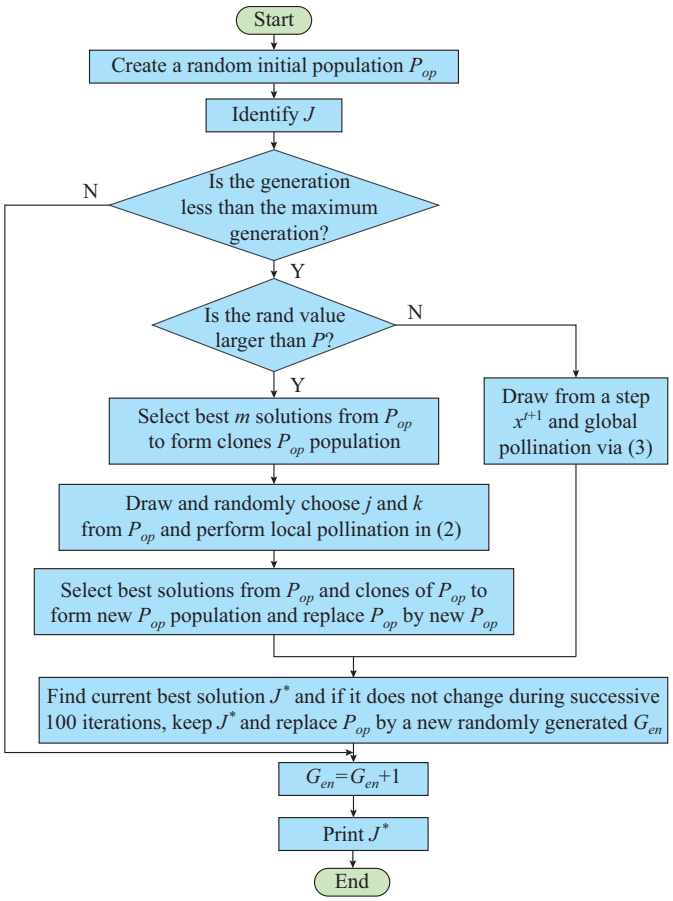

Fig. 5. Flowchart of MFPA optimization.

MPFA is used to determining the optimal two PI control parameters of the STATCOM for mitigating the ferroresonance overvoltage of DFIG-based WECS through minimizing ISE between the reference and actual voltage as presented in (1). Through 25 flowers and 100 iterations, the population of the flowers is initialized by a random selection of the four control parameters K_{pA}, K_{IA}, K_{pB}, and K_{IB} and positive values. Based on this random selection of the control parameters and the increasable voltage due to the ferroresonance, the objective function is determined for each flower and the global flower is selected from the populations in (2). For each flower, a random number is selected within the probability. Otherwise, the flower is randomly selected for local pollination. Pollinating the flower with global ones based on (3) is finished for each flower. For 100 iterations, all these processes are repeated, and the optimal four control parameters are recorded based on the minimum objective function.

C. Comparison of MFPA and PSO for Optimal Tuning of PI Control Parameters

To demonstrate the effectiveness of the proposed MFPA optimization technique for optimal tuning of the PI control parameters, another optimization technique namely particle swarm optimization (PSO) is considered for comparison. The PSO is stimulated by the behavior of some living organisms in groups like birds, fishes, and ants [32]. The PSO has had many applications in different optimization problems in power grid applications [30], [32], [33]. MFPA is proven to have higher efficiency than some other optimization techniques like PSO and harmony search for optimal tuning of PI control parameters for different applications [30], [33].

MFPA and PSO are compared through minimizing the objective function given in (1), the four PI control parameters using MFPA and PSO are given in Table I, and the convergence curves is presented in Fig. 6 for 100 iterations. The results show that MFPA provides better performance than PSO by reaching a lower value of the objective function that complies with the results presented in [30], [32], [33].

TABLE I
OPTIMAL PI CONTROL PARAMETERS USING MFPA AND PSO

Technique	K_{pA}	K_{IA}	K_{pB}	K_{IB}
MFPA	9	95	16	153
PSO	15	82	34	96

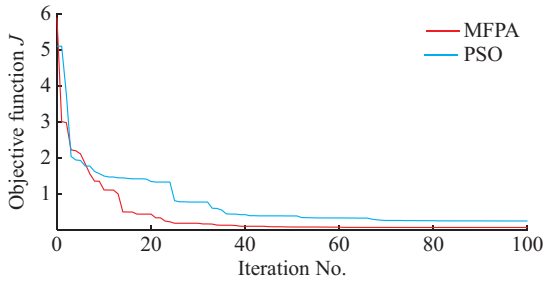

Fig. 6. Convergence curves for MFPA and PSO.

IV. RESULTS AND DISCUSSIONS

The grid-connected WECS is tested with and without installing the STATCOM when the ferroresonance occurs. Two cases are investigated including different services of the power transformer as follows.

A. Case 1: Ferroresonance Overvoltages of Isolated Transformer at Secondary side

The ferroresonance is simulated in this case, while the interconnection of the transformer of bus 1 is isolated as depicted in Fig. 1. The ferroresonance is initialized by disconnecting the pole of phase a of the breaker at point M. The voltage waveforms at the primary and secondary sides of the transformer of bus 1 and bus 2 are presented without using the STATCOM when the ferroresonance occurs are presented in Fig. 7(a) and (b), where the opening time of phase a for the breaker at point M is 1 s. The ferroresonance occurs frequently for positive and negative half-cycles as observed for the voltage measurements of bus 1 and bus 2. The ferroresonance increases the voltage of the opened phase instantaneously to 2.83 p.u. compared with the normal operation of pure rated voltage waveform before the ferroresonance occurs. The results confirm that the waveform distortion associated with high spikes is due to ferroresonance occurrence for each half-cycle. The current spikes in the no-load current of

the transformer increases from 0.01 to 0.1 p.u. due to the ferroresonances as depicted in Fig. 7(c).

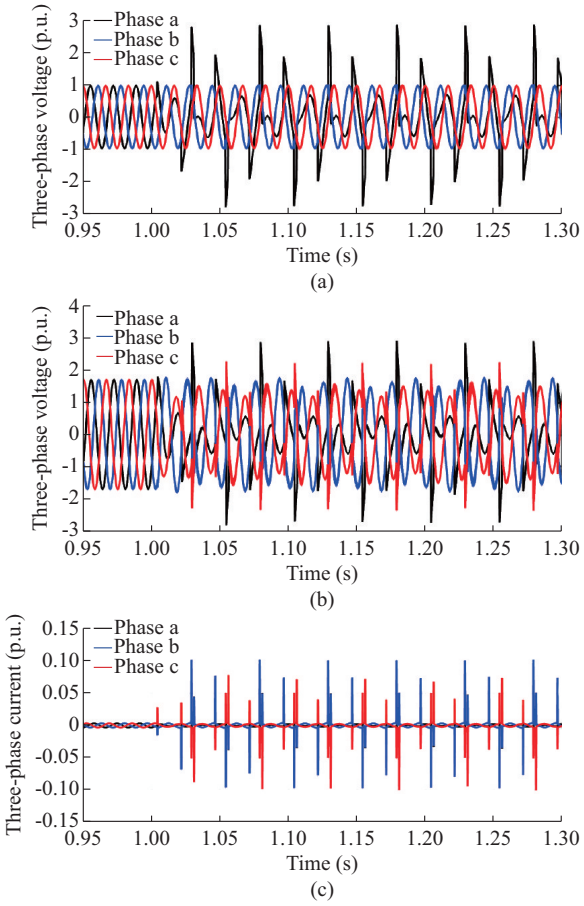

Fig. 7. Ferroresonance occurrence without STATCOM. (a) Three-phase voltage waveforms of bus 1. (b) Three-phase voltage waveforms of bus 2. (c) Three-phase current waveforms of bus 1.

When the controlled STATCOM is installed and evaluated toward mitigating the waveform distortion due to the ferroresonance occurrences as shown in Fig. 7, the corresponding voltage and current waveforms are improved as confirmed by the performance shown in Fig. 8. The STATCOM with the regulated power flow enhances and restores the voltage and current waveforms of the transformer to be pure sinusoidal ones. However, the open phase, which is a disturbance that could not be compensated using the STATCOM, still affects the voltage measurements,. The voltage of bus 1 is regulated at the level of 0.8 p.u. peak value due to the single-pole disconnection as depicted in Fig. 8(a). The voltage at the secondary side of the transformer of bus 2 is regulated at reduced levels due to the △ connection of this side as depicted in Fig. 8(b). Furthermore, the repetitive current spikes of the unloaded transformer disappear as shown in Fig. 8(c).

Due to the ferroresonance occurrence, the rotor speed increases by 16% which can damage the rotor shaft, and the speed values could not be retained to be lower value as depicted in Fig. 9. With the controlled the STATCOM, the rotor speed is slightly affected by the ferroresonance as concluded from the comparison shown in Fig. 9. The proposed STATCOM controller fast injects the reactive power from the STATCOM into the PCC to overcome the sudden increase of the voltage due to the ferroresonance as shown in Fig. 10.

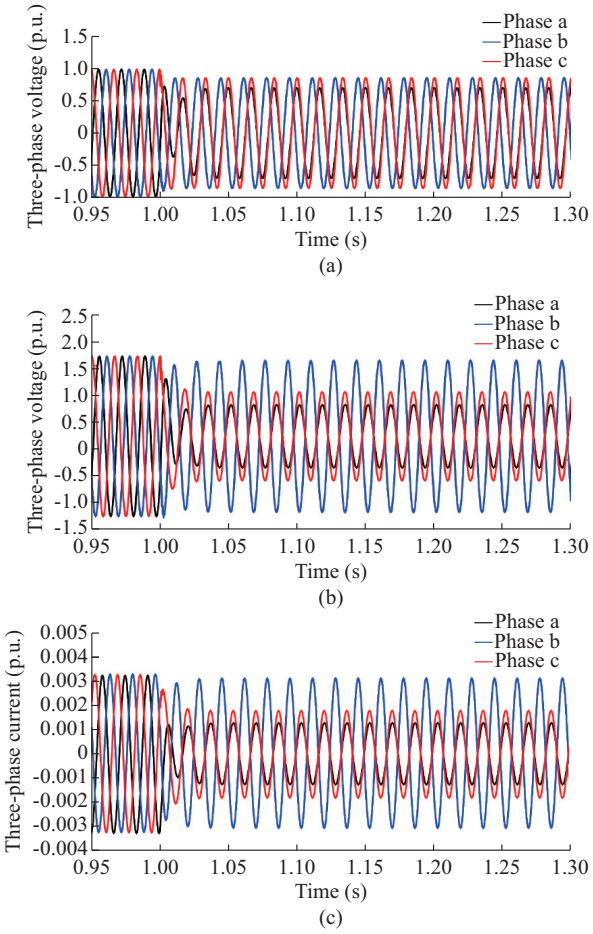

Fig. 8. Ferroresonance mitigation with STATCOM (case 1). (a) Three-phase voltage waveforms of bus 1. (b) Three-phase voltage waveforms of bus 2. (c) Three-phase current waveforms of bus 1.

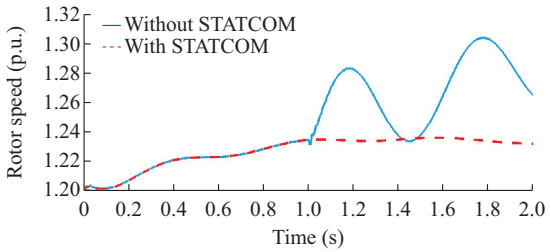

Fig. 9. Rotor speed of DFIG with and without STATCOM (case 1).

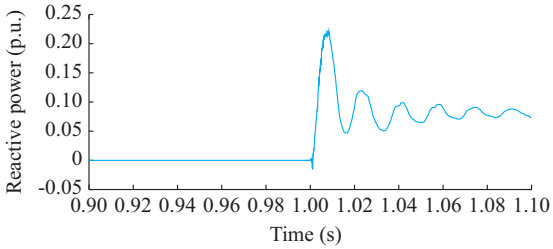

Fig. 10. Reactive power of STATCOM (case 1).

B. Case 2: Ferroresonance Overvoltage of In-service Transformer in Grid-connected WECSs

The pole of phase a of the breaker at point *N* of the transmission line connecting the WECSs into the power grid is opened at 1 s to simulate case 2. The ferroresonance is stimulated, while the transformer is in service to interconnect the WECSs into the power grid as shown in Fig. 1. Instantaneous voltage of PCC and bus 4 significantly increases to higher levels than 1 p.u. as depicted in Fig. 11(a) and (b), respectively. The current at PCC during the ferroresonance occurrence increases to 1.5 p.u. in a form of fundamental current as shown in Fig. 11(c). Comparing the currents in Figs. 7(c) and 11(c), the current of the open phase in Fig. 11(c) is significantly higher during the ferroresonance period, in which this high current path is through the non-linear inductance of the power transformer.

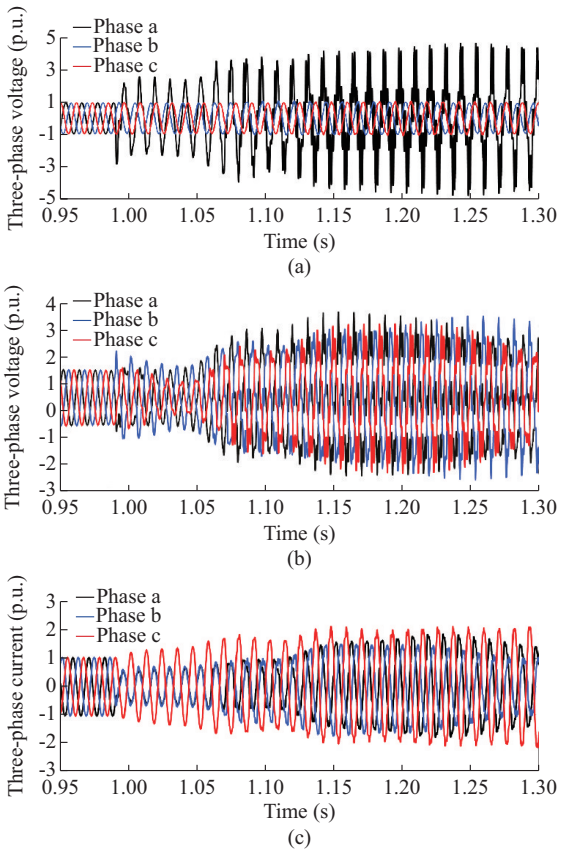

Fig. 11. Performance with ferroresonance occurrence. (a) Three-phase voltage waveforms at PCC. (b) Three-phase voltage waveforms at bus 4. (c) Three-phase current waveforms at PCC.

When the PI control parameters are optimized by MFPA and used to mitigate the ferroresonance overvoltage, the corresponding performance is shown in Fig. 12(a) and (b) for the measurements of the voltage at PCC and bus 4, respectively. The voltage of the transformers at PCC and bus 4 are affected owing to the single-pole opening of the breaker at point *N*. However, the voltage is not in the form of overvoltage owing to the fast regulation of the reactive power presented by the STATCOM. Furthermore, the current at PCC is reduced as shown in Fig. 12(c). The interrupted phase current is diminished. The STATCOM has dynamically protected the transformer from being damaged due to the ferroresonance overvoltage and overcurrent.

The optimal control of the STATCOM is attained to keep the rotor speed at a minimum disturbance compared with the speed values without using the STATCOM as shown in Fig. 13. The fast response of the reactive power from the controlled the STATCOM is shown in Fig. 14, in which it could mitigate the ferroresonance overvoltage and overcurrent.

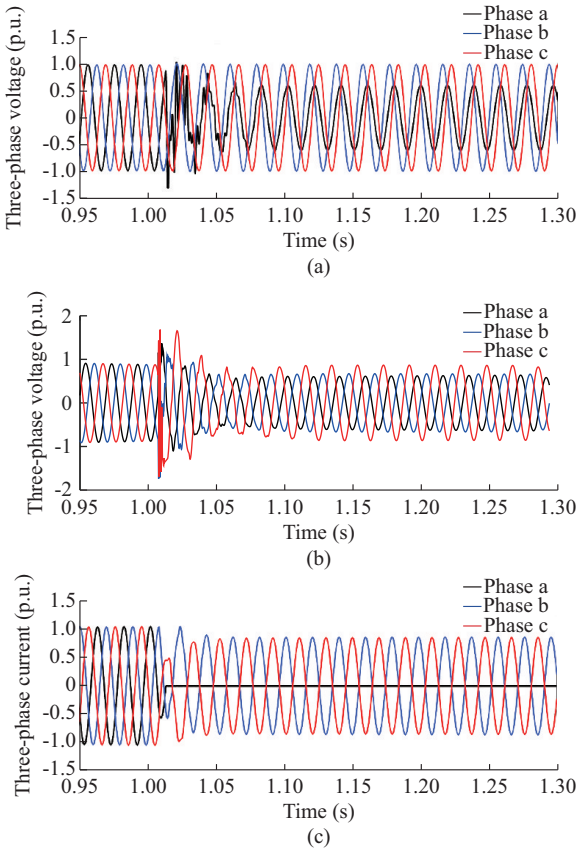

Fig. 12. Ferroresonance mitigation with STATCOM (case 2). (a) Three-phase voltage waveforms at PCC. (b) Three-phase voltage waveforms of bus 4. (c) Three-phase current waveforms of PCC.

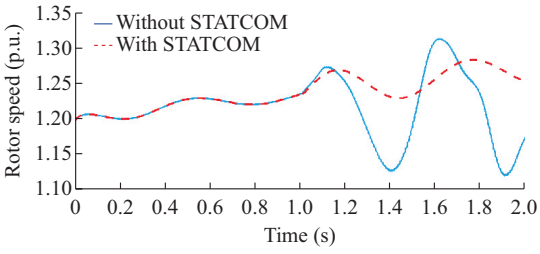

Fig. 13. Rotor speed of DFIG with and without STATCOM (case 2).

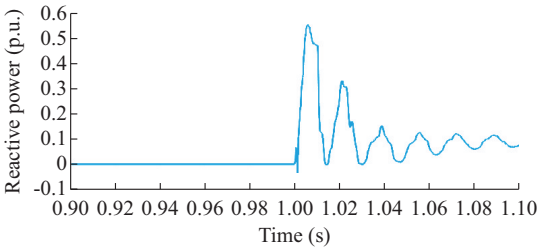

Fig. 14. Reactive power of STATCOM (case 2).

C. FFT-based Analysis

Ferroresonance modes are classified into four types: fundamental, subharmonic, quasi-periodic, and chaotic [34]. These types are recognized using the voltage or current spectra. There are many features indicating the ferroresonance occurrence [34], e.g., high permanent overvoltage and overcurrent. However, the overvoltage and overcurrent lead to catastrophic failure of the power grid. There are several modes for the ferroresonance interaction with the power grid. One of the methods processed to estimate the ferroresonance mode is the fast Fourier transform (FFT). Figure 15 shows FFT of the disturbed phase voltage for the aforementioned two test cases. Figure 15(a) and (b) illustrates the voltage waveforms of phase a for FFT shown in Fig. 7(a) and Fig. 11(a), respectively. FFT is numerically processed during the ferroresonance period using MATLAB. By comparing the spectrum and concerning the modes in [34], the ferroresonance of the case 1 is in a quasi-periodic mode, where there are frequencies f_2-f_1, f_1, f_2, $3f_1-f_2$, and nf_1+mf_2, where f_1 and f_2 are equal to 60 Hz and 80 Hz, respectively, and n and m are the integers as reported in [34]. However, case 2 refers to a chaotic mode with a fundamental dominant frequency. Figure 15(a) and (b) shows that the fundamental overvoltage of case 2 is higher than case 1 as the amplitude is higher.

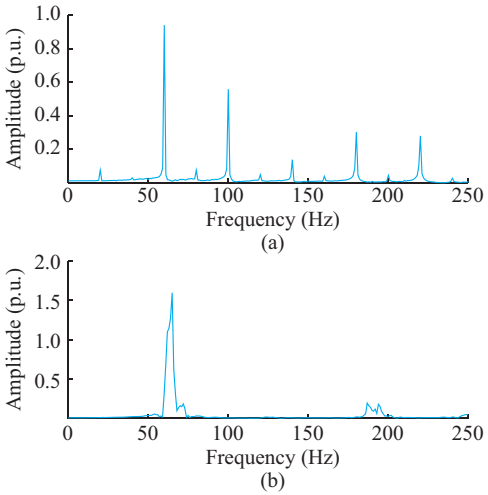

Fig. 15. FFT analyses of ferroresonance. (a) Phase voltage of case 1. (b) Phase voltage of case 2.

V. Conclusion

We introduce two PI controllers of the STATCOM using MFPA, where the interaction of STATCOM is successfully utilized to mitigate the ferroresonance phenomena of the DFIG-based grid-connected WECSs. The proposed optimal controllers mitigate the ferroresonance disturbances due to the rapid regulated injections or absorptions of the reactive power based on STATCOM. Accordingly, the system waveforms are restored to the sinusoidal shapes. However, the single-pole openning of the breaker has still caused a system disturbance. Considering the performance with DFIG, the voltage profile is improved and the generator rotor speed during ferroresonance phenomena is achieved successfully. By evaluating the ferroresonance overvoltage waveforms of grid-connected wind farm, the ferroresonance type is found as the quasi-periodic mode for the unloaded transformer and chaotic mode for the loaded transformer, in which it is numerically processed using FFT. In this paper, the ferroresonance occurrence is confirmed for the power transformer installed in the wind farms although they are fully in service. Accordingly, the mitigation method has been introduced using the STATCOM, which has efficiently mitigated the ferroresonace in the wind farms.

Appendix A

Tables AI and AII illustrate the parameters of induction machine and STATCOM rating data, respectively.

TABLE AI
Parameters of Induction Machine

Parameter	Value
Rated power	1.5 MW
Rated voltage	575 V
Rated frequency	60 Hz
Stator resistance	0.0045 Ω
Stator inductance	0.0357 H
Rotor resistance	0.0032 Ω
Rotor inductance	0.033 H
Mutual inductance	0.575 H

TABLE AII
Parameters of STATCOM

Parameter	Value
STATCOM rating	4 MVA
Series line resistance	0.1301 Ω
Series line reactance	2.42 Ω
DC-link capacitance	750 μF

References

[1] Y. Tang, H. He, J. Wen *et al*., "Power system stability control for a wind farm based on adaptive dynamic programming," *IEEE Transactions on Smart Grid*, vol. 6, no. 1, pp. 166-177, Jan. 2015.
[2] M. Mosaad, M. A. El-Raouf, M. Al-Ahmar *et al*., "Optimal PI controller of DVR to enhance the performance of hybrid power system feeding a remote area in Egypt," *Sustainable Cities and Society*, vol. 47, pp. 1-8, May 2019.
[3] J. Liua, Y. Lia, C. Rehtanz *et al*., "An OLTC-inverter coordinated voltage regulation method for distribution network with high penetration of PV generations," *Electrical Power and Energy Systems*, vol. 113, pp. 991-1001, May 2019.
[4] W. Hassanein, M. Ahmed, M. A. El-Raouf *et al*., "Performance improvement of off-grid hybrid renewable energy system using dynamic voltage restorer," *Alexandria Engineering Journal*, vol. 59, no. 3, pp. 1567-1581, Jun. 2020.
[5] Y. Gounder, D. Nanjundappan, and V. Boominathan, "Enhancement of transient stability of distribution system with SCIG and DFIG based wind farms using STATCOM," *IET Renewable Power Generation*, vol. 10, no. 8, pp. 1171-1180, Sept. 2016.
[6] M. Mosaad, "Model reference adaptive control of STATCOM for grid integration of wind energy systems," *IET Electric Power Applications*, vol. 12, no. 5, pp. 605-613, May 2018.
[7] J. Ruan, Z. Lu, Y. Qiao *et al*., "Analysis on applicability problems of the aggregation-based representation of wind farms considering DFIGs' LVRT behaviors," *IEEE Transactions on Power Systems*, vol.

31, no. 6, pp. 4953-4965, Nov. 2016.
[8] M. Mosaad, "Direct power control of SRG-based WECSs using optimised fractional-order PI controller," *IET Electric Power Applications*, vol. 14, no. 3, pp. 409-417, Mar. 2020.
[9] N. Hingorani and L. Gyugyi, *Understanding FACTS Concepts and Technology of Flexible AC Transmission Systems*, New York: Wiley-IEEE Press, 2000.
[10] M. Mosaad, A. Abu-Siada, and M. Elnaggar, "Application of superconductors to improve the performance of DFIG-based WECS," *IEEE Access*, vol. 7, no. 1, pp. 103760-103769, Jul. 2019.
[11] Y. Alharbi, A. Yunus, and A. A. Siada, "Application of UPFC to improve the LVRT capability of wind turbine generator," in *Proceedings of 22nd Australasian Universities Power Engineering Conference* (*AUPEC*), Bali, Indonesia, Sept. 2012, pp. 26-29.
[12] A. Abdou, H. Pota, A. Abu-Siada *et al*., "Application of STATCOM-HTS to improve DFIG performance and FRT during IGBT short circuit," in *Proceedings of Australasian Universities Power Engineering Conference (AUPEC)*, Perth, Australia, Sept. 2014, pp. 1-5.
[13] C. Wessels, N. Hoffmann, M. Molinas *et al*., "STATCOM control at wind farms with fixed-speed induction generators under asymmetrical grid faults," *IEEE Transactions on Industrial Electronics*, vol. 60, no. 7, pp. 2864-2873, Jul. 2013.
[14] M. Navaei, A. Abdoos, and M. Shahabi, "A new control unit for electronic ferroresonance suppression circuit in capacitor voltage transformers," *Electrical Power and Energy Systems*, vol. 99, pp. 281-289, Jul. 2018.
[15] M. Yang, W. Sima, L. Chen *et al*., "Suppressing ferroresonance in potential transformers using a model-free active-resistance controller," *Electric Power and Energy Systems*, vol. 95, pp. 384-393, Feb. 2018.
[16] T. Mellik, F. Painter, D. Shipp *et al*., "Proactive study and novel mitigation of MV power system damage due to sub-power-frequency ferroresonance for a gas plant," *IEEE Transactions on Industry Applications*, vol. 54, no. 4, pp. 3991-4000, Jul. 2018.
[17] Y. Wang, X. Liang, I. Pordanjani *et al*., "Investigation of ferroresonance causing sustained high voltage at a de-energized 138 kV bus: a case study," *IEEE Transactions on Industry Applications*, vol. 55, no. 6, pp. 5675-5686, Nov. 2019.
[18] E. Bayona, F. Azcondo, C. Brañas *et al*., "Electronic resistor emulators forferroresonance damping in MV transformers," *IET Renewable Power Generations*, vol. 13, no. 1, pp. 201-208, Jul. 2019.
[19] U. Karaagac, J. Mahseredjian, and L. Cai, "Ferroresonance conditions in wind parks," *Electric Power Systems Research*, vol. 138, pp. 41-49, Sept. 2016.
[20] H. Radmanesh and G. Gharehpetian, "Ferroresonance suppression in power transformers using chaos theory," *Electric Power and Energy Systems*, vol. 45, no. 1, pp. 1-9, Feb. 2013.
[21] H. Radmanesh, "Distribution network protection using smart dual functional series resonance-based fault current and ferroresonance overvoltage limiter," *IEEE Transactions on Smart Grid*, vol. 9, no. 4, pp. 3070-3078, Jul. 2018.
[22] H. Fordoei, H. Heydari, and S. Afsari, "Elimination of chaotic ferroresonance in power transformer by ISFCL," *Electrical Power and Energy Systems*, vol. 68, pp. 132-141, Jun. 2015.
[23] A. Akinrinde, A. Swanson, and R. Tiako, "Dynamic behavior of wind turbine generator configurations during ferroresonant conditions," *Energies*, vol. 12, no. 4, pp. 1-12, Feb. 2019.
[24] M. Siahpoosh, D. Dorrell, and L. Li, "Ferroresonance assessment in a case study wind farm with 8 units of 2 MVA DFIG wind turbines," in *Proceedings of 20th International Conference of Electrical Machines and Systems (ICEMS)*, Sydney, Australia, Aug. 2017, pp. 1-5.
[25] J. Marti and A. Soudack, "Ferroresonance in power systems: fundamental solutions," *IEE Proceedings: Generation, Transmission and Distribution*, vol. 138, no. 4, pp. 321-329, Jul. 1991.
[26] S. Mohod and M. Aware, "A STATCOM-control scheme for grid connected wind energy system for power quality improvement," *IEEE Systems Journal*, vol. 4, no. 3, pp. 346-352, Sept. 2010.
[27] Y. Zhang, M. Cheng, and Z. Chen, "Load mitigation of unbalanced wind turbines using PI-R individual pitch control," *IET Renewable Power Generation*, vol. 9, no. 3, pp. 262-271, Apr. 2015.
[28] F. Freijedo, A. Vidal, A. Yepes *et al*., "Tuning of synchronous-frame PI current controllers in grid-connected converters operating at a low sampling rate by MIMO root locus," *IEEE Transactions on Industrial Electronics*, vol. 62, no. 8, pp. 5006-5017, Aug. 2015.
[29] M. Mosaad and F. Salem, "Adaptive voltage regulation of self-excited induction generator using FACTS controllers," *International Journal of Industrial Electronics and Drives*, vol. 1, no. 4, pp. 219-226, Dec. 2014.
[30] M. Mosaad and H. Ramadan, "Power quality enhancement of grid-connected fuel cell using evolutionary computing techniques," *International Journal of Hydrogen Energy*, vol. 43, no. 25, pp. 11568-11582, Jun. 2018.
[31] E. Nabil, "A modified flower pollination algorithm for global optimization," *Expert System Application*, vol. 57, pp. 192-203, Sept. 2016.
[32] W. Ongsakui and P. Jirapong, "Optimal allocation of FACTS devices to enhance total transfer capability using evolutionary programming," in *Proceedings of IEEE International Symposium on Circuits and Systems*, Kobe, Japan, May 2005, pp. 23-26.
[33] M. Mosaad, A. Alenany, and A. Abu-Siada, "Enhancing the performance of wind energy conversion systems using unified power flow controller," *IET Generation, Transmission & Distribution*, vol. 14, no. 10, pp. 1922-1929, May 2020.
[34] P. Ferracci. (1998, Mar.). Ferroresonance Cahier Technique Schneider no. 190, the Groupe Schneider's. [Online]. Available: https://www.studiecd.dk/cahiers_techniques/Ferroresonance.pdf

Mohamed I. Mossad received the B. Sc. and M. Sc. degrees from Zagazig University, Zagazig, Egypt, and the Ph. D. degree from Cairo University, Cairo, Egypt, all in electrical engineering. Currently he is an Associate Professor in the Department of Electrical and Electronic Engineering Technology, Yanbu Industrial College (YIC), Yanbu, Saudi Arabia. He is the Editor-in-Chief for Yanbu Journal of Engineering and Sciences (YJES). His research interests include power system stability, control and renewable energy.

Nehmdoh A. Sabiha received the B.Sc. (first class honors) and M.Sc. degrees in electrical engineering from Faculty of Engineering, Menofia University, Shebin Elkom, Egypt, in 2002 and 2006, respectively. She received the D.Sc. degree in technology from Aalto University, Espoo, Finland, in 2010. Currently, she is an Assistant Professor at Menofia University. However, she is in absence leave to work at Taif University, Taif, Saudi Arabia. Her research interests include high-voltage engineering, overvoltage protection of renewable energy farms concerning transients and ferroresonance mitigations, nanotechnology applications in high-voltage engineering, and cathodic protection.